WAAM processing of AISI 410 stainless steel for part building

João Miguel Araújo Bruno

jmabruno.10@gmail.com

Instituto Superior Técnico, Universidade de Lisboa, Portugal

November 2019

Abstract

Wire and Arc Additive Manufacturing (WAAM) is an additive manufacturing process that is receiving increased attention from researchers and manufacturers. Making use of standard welding equipment, studies have shown that there is possibility that this process reveals itself to be quite an attractive replacement or complement for certain traditional manufacturing processes and thus carving its place in the 4th industrial revolution.

In this work, the feasibility of using a low carbon martensitic stainless steel, AISI 410, for WAAM processing using a CMT power source was investigated. After an initial stage of parametrization work, material characterization tests, namely, metallographic analysis, hardness tests and tensile tests, were performed and compared to the expected values found in literature and manufacturer technical data sheets. Microstructure and hardness were found to be in line with what was found in specialized literature, with metallographic analysis not revealing any of the common defects associated with martensitic structure. Tensile testing revealed that tensile properties were anisotropic, with samples perpendicular to direction of deposition showing greater strength (1235,15 MPa vs 1122,42 MPa), and samples parallel to direction of deposition showing greater ductility (0,10 vs 0,07). After parametrization and material characterization, two CAD software's, Autodesk's PowerMill Additive and Cranfield's University WAAM Software, WAAMPlanner, were used for part deposition and the subsequent results were analyzed. Finally, a final part was deposited based on the best parameters and deposition strategy.

It has been shown that, using WAAM processing, it is possible to use a CAD software to design and deposit a part with high hardness and tensile strength, especially attractive properties to parts requiring high resistance to wear while in use.

Keywords: Wire and Arc Additive Manufacturing, DED+Arc, WAAM, AISI 410, martensitic stainless steel, CMT, WAAM Software, deposition strategies

1. Introduction

In today's world, where industrial competition, locked in an ever-growing state, is faced with an increasingly environmentally conscious society, an economic pressure that forces manufacturers to do "more with less" and consumers demand for customized items, the need to reduce both costs and material waste while keeping a flexible manufacturing approach has reached an all-time high. As a response to this need, Additive Manufacturing (AM) processes have begun to arise. Considered little more than a novelty when it first emerged, AM processing of materials have begun to find their place in the industrial environment, promising personalized items at no increased cost, shortening of supply chains and reduction of material waste [1], [2].

Being one of the cornerstones of engineering applications, AM techniques for the processing of metals have been and are being research as of now, seeking to take advantage of the benefits brought by this technology. Among

these techniques, Directed Energy Deposition (DED), and, more specifically Wire and Arc Additive Manufacturing (WAAM), is one that shows promise in an industrial environment. Being an arc-based process and using metallic wire as feedstock, this process builds upon vastly researched welding processes in an attempt to build increasingly complex parts while enjoying high deposition rates, reduced material waste and ease of access to the process itself [3].

When all of these factors are considered, it comes as no surprise that research in WAAM and AM in general is being increasingly researched and, expanding the range of materials that can be used by this technology will only lead to a larger field of applications. This is why there is a drive in researching this subject and contribute to the advancement of the manufacturing industry. The feasibility of using a low carbon variant of an AISI 410 stainless steel for CAD assisted fabrication of parts by WAAM processing is the focus of this paper.

Being a martensitic stainless steel, it is expected that the material used in this work displays high wear resistance. Due to this nature, it is relevant to analyze the current studies on wear resistance of parts manufactured by WAAM. Although no study on WAAM processed AISI 410 was found, Amrei *et al.* [4] carried out a study on multipass welding for this material. They observed a complex and heterogeneous microstructure, with several regions affected by adjacent weld beads, which also led to a variation of hardness values across the weld beads, with values ranging from 340 HV to 400 HV.

Wang *et al*. [5] studied the properties of AISI H13 steel and discovered that, for thin walled structures, Vickers hardness was kept uniform across the height of the samples, assuming values between 300 and 360 HV, high values that correlate to a high wear resistance for this material.

Xu *et al.* [6] studied the deposition of a MARVAL 18S maraging steel by WAAM. They observed that a significant difference in hardness, from 330 HV at the bottom to 430 HV at the top, was present along the height of the part, due to the aging effect from each successive deposition. This difference was eliminated after aging the part and the hardness value increased, reaching 550 HV, suggesting that incorporating aging treatment could be very beneficial to the production of wear resistant steel parts. As for tensile properties, a UTS of 1165 MPa and an elongation of 13,7% were observed.

Having in consideration that one of the main objectives of this work is the construction of a part by WAAM, deposition strategies are of paramount importance in order to produce defect free parts. One of the most evident issues when depositing single walls is when the starting and ending height present a considerable difference between them. This happens when the start and end point is the same for every layer, where excessive heat sink at the initial deposition point causes lack of weld penetration, creating an increase in layer height. On the opposite side at the final deposition point, low heat dissipation, due to the high temperatures associated with the welding process, cause a drop in layer height [7]. This error will be accumulating throughout the building process, creating a considerably large difference between extremities. Two methods are currently employed to overcome these differences. One of them is to control the current employed in the process and travel speed of the torch, increasing them at the starting deposition point and reducing them at the end point [8]. The other method employs a “zig-zag” motion of the torch where the start and end point of deposition changes with every layer [9]. This method also solves the problem in a satisfactory manner, but it can also result in high residual stresses at the wall boundaries, due to thermal accumulation in certain zones [7]. A workaround for this geometric inconsistency can be considering the starting and ending areas as sacrificial zones to be removed.

Understanding weld bead geometry and its relation to the process parameters is also of extreme importance to obtain a defect free part. Researchers have tried to correlate welding parameters and bead geometry by regression analysis [10], artificial neural networks or combinations of these two techniques [11]. Researchers have determined that the optimal model of bead profile was dependent of the ratio

between wire feed speed and travel speed of the torch, by comparing measured weld bead deposited with different welding parameters with three bead profile models [12].

Another study was carried out where the effect of three different deposition strategies on surface waviness and porosity in steel was carried out [13]. The three strategies were oscillation, parallel and weaving). In this study it was determined that employing a weaving strategy not only resulted in a better surface finish, with a flatter top, which requires less machining after deposition, but also led to a decrease in porosity in the welds.

Regarding the decomposition of CAD models, studies seeking to minimize the number of start and stop of the torch and weld intersections have been carried out. One of them decomposed layers in polygons, filling each area and generating a closed loop toolpath [14]. Another method that has been developed, where the geometry of a slice plane is divided in a set of bisector segments. When these segments connect at more than two points they become branch points, with the depositions paths being generated around the segments connected by them [15].

The manufacturing of 90º walls has also been investigated. The developed strategy consisted in applying two complementary strategies, building four layers with the first one and using the second one to correct the geometry [16].

2. Methods and Materials

2.1 Materials

The material used for this work was a martensitic stainless steel, OK Autrod 410NiMo. It was supplied in wire form, by ESAB, with a diameter of 1.2 mm, in a 15 Kg spool. Like all martensitic steels, AISI 410 possesses high corrosion resistance, high strength and high toughness. Due to its low carbon content of 0.02% it is considered a supermartensitic stainless steel and it is used in various industries for the fabrication of essential parts, such as parts for computer hard drives, plastic moulds, screws, valves, shafts, bearings and pipelines as an alternative to austenitic and duplex stainless steels [17].

2.2 Equipment Setup

The deposition work was performed at IST using a 6-axis KUKA robot coupled with a Fronius CMT welding power source. The shielding gas used for the deposition work was ARCAL Chrome with a mixture of Ar+2%CO_2 – ISO 14175-M12-ArC-2. The substrates were clamped to a steel table. The setup is presented in Figure 1. The labeling of the figure is: 1 - KUKA Robot, 2 - Torch, 3 - KUKA Robot Controller, 4 - CMT Power Source Controller, 5 - Wire Feeder, 6 - CMT Power Source, 7 - Shielding Gas Bottle, 8 - Exhaust Ventilation System, 9 - Substrate, 10 – Clamps.

Figure 1 Deposition work setup

2.3 Deposition Parameters

Two sets of depositions were carried out in order to determine the process parameters to be used to produce a more complex part.

The first set of experiments consisted in single bead walls with six layers each and 100 mm in length, created with a zig-zag motion of the torch, meaning that the start point changes with every consecutive layer. The followed methodology for this deposition was to vary one parameter, while keeping all the others constant, in order to ascertain the effect that parameter has on the quality of the deposition.

The Shielding Gas Flow Rate (SGFR) and Contact Tip to Work Distance (CTWD) were kept constant throughout all depositions. The Wire Feed Speed (WFS) was varied in a range of values allowed by the welding machine controller. The other varied parameter was the Travel Speed (TS) of the torch, computed from a range of ratios WFS/TS. The current and voltage were set automatically by the welding machine, and its values were dependent on the

selected material curve and WFS set on the controller.

The second set consisted in walls created with an oscillation strategy, also with 6 layers and 50 mm in length. This second study was carried out after verifying the parameters defined previously for the single bead walls, are not suitable when producing walls with an oscillation strategy. Therefore, the same methodology was followed to determine a new set of parameters that could provide a solution to these problems.

These depositions were measured with a set of calipers. Three measurements were taken in order to calculate average width and thickness, two of them near the extremities and the other one in the center.

2.4 Metallographic Analysis

The metallographic analysis was carried out at Instituto de Soldadura e Qualidade (ISQ). The samples for metallographic analysis were hot mounted into cylinder moulds using a Struers LaboPress-3 machine. The samples were grinded with various grit size sandpapers, ranging from 80 grit size to 1000 grit size, using a Struers Labopol. With the same equipment, the samples were polished with two different cloths and an abrasive agent. Finally, the samples were etched with Villela reagent by an ISQ member. The microstructure was then investigated under an optical microscope while a conventional scanner machine was used to obtain the macrostructure.

2.5 Hardness Tests

Hardness indentations were made with a Struers Duramin available at IST. The indentations were performed under a load of 5 N for 10 s per point in different zones of the samples along the height of the sample, obtaining 10 points per sample, spaced 1 mm between them, while also taking points from the Heat Affected Zone (HAZ). With the hardness measurements it is also possible to estimate the Ultimate Tensile Strength (UTS) and Yield Strength (YS) of the deposited material. The values for UTS and YS can be estimated from the Vickers Hardness (HV) values through experimental correlations.

2.6 Tensile Tests

Tensile tests were made with an INSTRON Universal Testing Machine with a 200 kN cell available at the mechanical testing laboratory at IST. The elongation was measured by an extensometer placed on tensile specimens. Tests were performed with a load speed of 1 kN/min, following a ramp function, until reaching yield stress, and afterwards a constant speed of 5 mm/min until finishing the test. Two sets of walls were deposited in order to extract samples in both orientations. The samples were manufactured according to the ISO 6892-1:2016 standard. Two longitudinal (parallel to deposition direction) and four transversal samples (perpendicular to deposition direction) were removed from each wall.

2.7 Deposition Parameters and Procedure for Part Construction

This part was designed with challenge in mind rather than actual functionality, meaning that a set of somewhat challenging geometries for WAAM processing were selected and combined into a single part in order to determine the best strategies and process parameters that would lead to a successful build of these geometries using this material. Figure 2 shows the part that was designed.

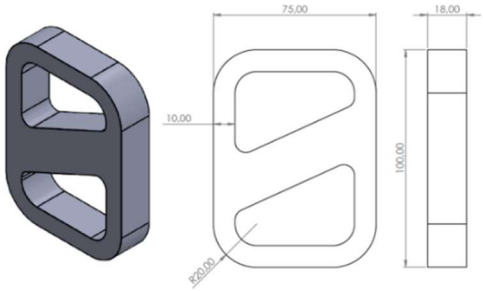

Figure 2 Model and technical drawing of the part

The deposition of the parts was carried out using two different software's, Autodesk's PowerMill Additive and WAAMPlanner.

3. Results and Analysis

3.1 Deposition Parameters

Figure 3 shows the results of the first set of depositions, which consisted in sixteen linear depositions.

Figure 3 First set of depositions

After measuring the resulting depositions, a visual analysis of each wall was performed. Figure 4 shows the visual evaluation of the walls.

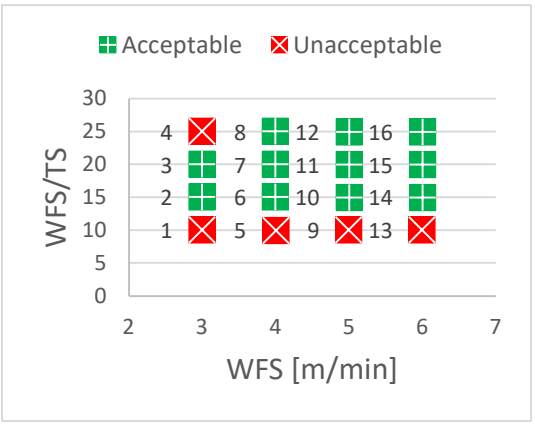

Figure 4 Visual evaluation of first set of depositions

From Figure 4 it can be seen that, with the exception of the experiments pertaining to WFS/TS ratios of 10 (1, 5, 9, 13) and experiment 4, all other experiments are classified as acceptable. Acceptable depositions are those which do not show any glaring defects, such as excess or lack of material in any given area or deviations in their measurements visible to the naked eye. Experiences 1, 5, 9 and 13 were classified as unacceptable because they do not provide depositions with enough height due to their high TS. Experiment 4 was classified as unacceptable because the extremities of the bead showed a significant drop in height due to the low WFS used which could not provide enough material to fill that part of the weld bead.

Figure 5 shows the average values for width and height for each experiment.

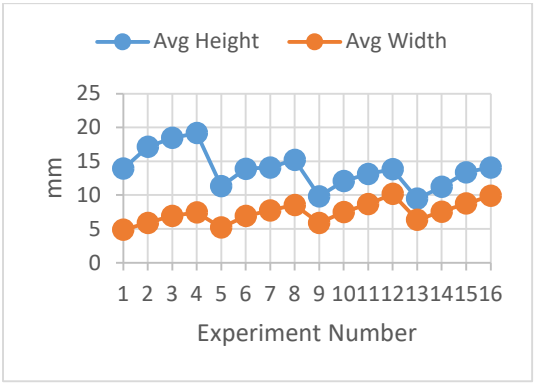

Figure 5 Average width and height of depositions

Observing Figure 5 it can be seen that the width of the deposits, for the same value of WFS, increases with the WFS/TS ratio. This is expected behaviour since increasing WFS/TS means reducing the TS of the torch, introducing more material into the melt pool. For the same reason, increasing the WFS also leads to larger bead width for the same WFS/TS ratio, although in a smaller magnitude. The average height of each bead increases when the WFS/TS ratio is increased and the WFS is kept constant, as expected, also due to more material being deposited per unit of length which allows for the height to build up quicker.

A second set of experiments was carried out with the purpose of determining the best parameters that would allow for defect free depositions when employing an oscillation strategy using WAAMPlanner. The resulting experiments are presented in Figure 6.

Figure 6 Second set of depositions

These experiments were also measured and visually inspected like the previous ones. The visual inspections are presented in Figure 7.

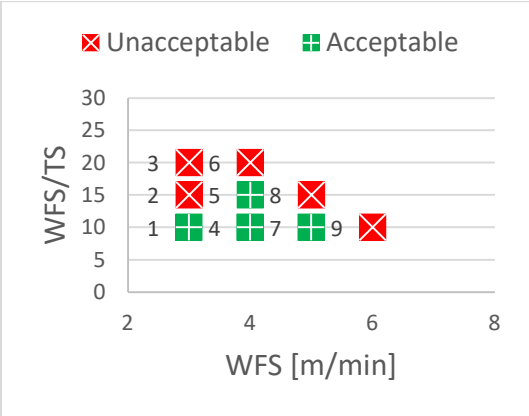

Figure 7 Visual evaluation of second set of depositions

From Figure 7 it can be seen that experiments 1, 4, 5 and 7 are classified as acceptable, following the same criteria from the previous set of experiments. The remaining experiments present, at least, one of such defects, which earns them the classification of unacceptable and excludes them from the list of parameters to be tested during part deposition.

The measurements of these experiments were used to calculate percentage of deviation, allowing us to identify the most regular depositions. Figure 8 shows the percentage of deviation for each experiment performed.

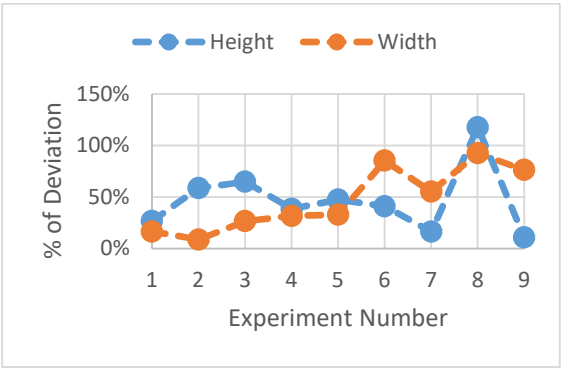

Figure 8 Percentage of Deviation comparison by experiment

Figure 8 shows that experiments 1, 4 and 5 offer the best balance between height and width, with experiment 1 showing the smallest values of percentage of deviation, making them candidates for the final part deposition.

This preliminary deposition work allowed for the determination of a set of parameters that yielded depositions that were, not only regular, but also had adequate mechanical properties and microstructures, which in turn allowed for the production of parts that met the required objectives.

3.2 Metallographic Analysis

In Figure 9 the microstructure of a section of a wall is presented. In the same figure it can be observed the gradient of microstructure along the wall, in which can be distinguished the first layers (Figure 9 – (a)), HAZ (Figure 9 – (b)), start of the columnar region (Figure 9 – (c)) and the last layers (Figure 9 – (d)), where it is observed a well-known grain morphology of AM parts, a columnar region aligned along the buildup direction, following the heat flow direction towards the surface of each bead.

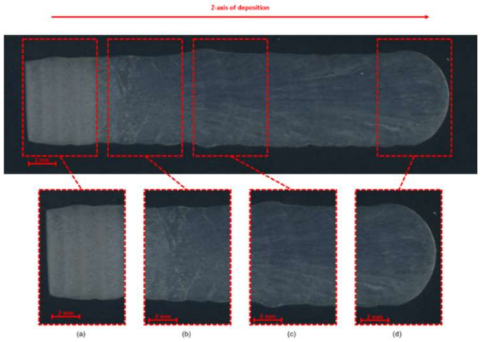

Figure 9 Macrostructure of a section of a deposition

During microscopic observation of the sample none of the common welding defects, such as cracks, porosity or lack of fusion were detected. Figure 10 shows the microstructure in different sections of the sample.

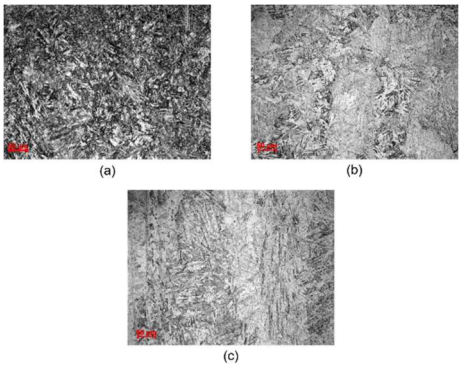

Figure 10 Microstructure in (a) - bottom portion of the sample, (b) - middle portion of the sample, (c)- top of the sample

Observing Figure 10 – (a) a nearly fully martensitic microstructure is visible. With 0,91 of $\%C_{eq}$, a mixture of lath and plate martensite was expected. Some amounts of retained

austenite can also be discerned, which, being softer than martensite, leads to a decrease in hardness and an increase in ductility. Figure 10 – (b) shows a mixture of tempered and freshly formed martensite. The martensite present in this section of the sample shows a finer microstructure than the one present in Figure 10 – (a). Carbides can also be observed, showing as small round dots. Grain size also shows an increase in dimension due to the additional thermal cycles. Figure 10 – (c) shows regions with column shaped microstructure and fine martensite microstructures. This column shaped microstructure follows the direction of the heat flow towards the top of the sample. Carbides are also visible in these micrographs. Like expected, successive thermal cycles increased grain size even further when compared with the previous analyzed section.

3.3 Hardness Tests

Table 1 shows the Vickers hardness values for the analyzed samples and the values for UTS and YS calculated from the following experimental correlations.

Table 1 Values for Vickers Hardness, UTS and YS

Variables	Samples				
	1	2	3	4	5
Avg Vickers Hardness [HV]	412	412	405	372	400
UTS [MPa]	1437	1440	1413	1291	1395
Average UTS [MPa]	1395				
YS [MPa]	1093	1095	1074	980	1061
Average YS [MPa]	1061				

Showing average values for Vickers Hardness between 372 HV and 412 HV for the tested samples, never has the value of 450 HV for the “as welded” condition, determined in [18], been reached. This is related with the constant reheating of the sample with every successive layer, which leads to coarser grain size, which in turn leads to a decrease in hardness. The hardness was found to be independent of the process parameters used in the manufacturing of the samples. The average values for UTS and YS were 1394,99 MPa and 1060,62 MPa, respectively, which are superior to the values for UTS and YS supplied by the manufacturer, (1050 MPa and 860 MPa, respectively for the “as welded” condition), and outside the standard errors defined for these correlations.

3.4 Tensile Tests

The tensile tests performed for both the transversal (perpendicular to the direction of deposition) and longitudinal (parallel to the direction of deposition) samples are presented in Table 2. Samples T1 to T3 pertain to the transversal tensile specimens while samples L1 and L2 pertain to longitudinal tensile specimens. For comparison, data from the manufacturer regarding the typical tensile properties of this material as welded is also presented.

Table 2 YS, UTS and Strain to fracture determined by tensile testing

	Tensile Properties		
Samples	YS 0,2% [MPa]	UTS [MPa]	Strain
T1	970	1226,44	0.06
T2	941	1235,12	0.07
T3	949	1223,75	0.06
L1	887	1091,89	0.10
L2	842	1122,42	0.08
As welded	860	1060	0.13

Figure 11 shows the true stress-strain curve until necking of samples T3 and L1.

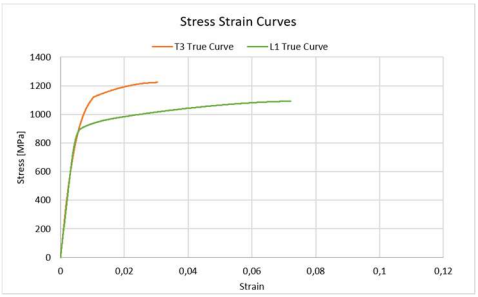

Figure 11 True stress-strain curves of samples T3 and L1

From Table 2 and Figure 11 we can observe that transversal samples offer a higher degree of tensile strength than longitudinal samples (1235,12 MPa vs 1122,42 MPa), while longitudinal samples offer a considerably greater degree of ductility (0,10 vs 0,07). This difference suggests that thermal history has a significant impact on material properties. Comparing the values obtained from tensile testing with the ones obtained from hardness correlations we can observe that, although still outside the standard error for UTS, they show a closer relationship than when compared with the values supplied by the manufacturer.

3.5 Part Deposition

Like mentioned previously two software's were used and compared for depositing parts. Figure 12 shows the resulting depositions made with Autodesk PowerMill Additive.

Figure 12 Experiments performed for the part deposition with PowerMill Additive

Irregular shapes, with severe variations in dimensions in the different segments of the part, deficient connection between them, irregular corners with excess material buildup and differences in height in different sections of the part were the most severe defects found while depositing with this software. Having a more automated approach doesn't allow for much control of deposition paths. Figure 13 shows the resulting depositions made with WAAMPlanner.

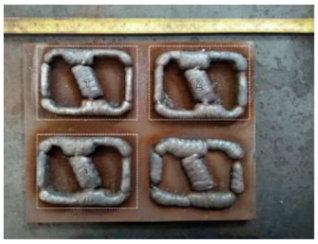

Figure 13 Experiments performed for part deposition with WAAMPlanner

The most obvious defect is lack of connection between segments. Although excess material accumulation near the corners and in the intersection of the middle and outer section has also been observed. Nevertheless, the shape of the deposited parts shows more regularity when compared with PowerMill's. This software also allows for more control of the deposition path and local parameters, therefore it was chosen for the deposition of the final part.

For the deposition of the final part two issues required attention, the lack of connectivity between segments and the buildup of material in the corners of the part. In order to improve segment connectivity two approaches were tested, increasing overlap between the segments by adjusting the deposition path and lowering the TS of the torch in these areas in order to provide more material per unit of area and close the gaps. After testing both options, it was verified that maintaining a constant TS and optimizing the deposition path was a more viable approach. In order to reduce excess material buildup in the corners of the part, it was first attempted to use the strategy of the first experiment with the increased overlap between segments, while increasing the TS of the torch to compensate the slowing down of the robotic system linear velocity when performing a curvilinear movement, depositing less material per unit of area as a consequence. After testing and concluding that this approach didn't offer significant improvements, new strategies for deposition path were attempted.

During deposition of the final part it was observed that the characteristics of the experiment that served as base for this deposition, are mostly maintained with the increase in height. It was observed that the corners and linear segments of the part retain their regularity, the connection between segments is complete, without visible gaps between them. Nevertheless, the increase in height caused the accumulation of the excess material buildup in the Z direction that was present before. Another defect introduced indirectly by the increase in height is presented in Figure 14.

Figure 14 Defect on final part

In Figure 14 it's visible that the middle section has collapsed. Like stated before this defect was introduced indirectly by the increase in height, since the additional thermal cycles created by it led to lower thermal gradients and, consequently, higher heat accumulation. This heat accumulation increased the solidification time of the metal, which led to its collapse. The reason why this defect is not present in other areas of the part is that a higher amount of material is deposited in this section. To solve this defect, the waiting time between layers was

increased, to allow for more cooling. In order to control the temperature between each successive layer deposition a Hanna HI 935005 thermocouple thermometer was used. The interlayer temperature was kept at around 200 ºC. The parameters and deposition path remained the same as the previous attempt. The resulting deposition is presented in Figure 15 and Figure 16.

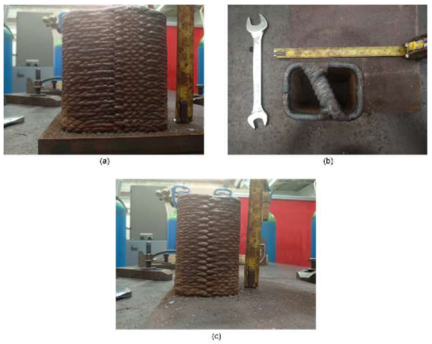

Figure 15 Final part (a) – front view, (b) – top view, (c) – side view

Figure 16 Area of the previously observed defect

Observing Figure 15 it can be seen that the geometric characteristics of the previous attempt are still present even with the further increase in height. During deposition it was observed that excess of material buildup in Z could be fixed by introducing “corrective segments” every two consecutive layers, meaning different segments from the regular ones which would level the top layer of the part. It would be advantageous if the software could take this into account, perhaps by allowing the creation of a “sublayer” after a consecutive number of user defined layers where these corrective segments could be introduced, similarly to the strategy outlined in section 1 for the manufacturing of 90º walls.

Figure 16 shows that controlling the interlayer temperature corrected the defect that was present in the previous attempt of final part deposition, without any visible material collapse. This temperature control was also employed between segments, since the deposition of material also heats up the zone adjacent to it. This intersegment temperature control was especially relevant when depositing the middle section of the part.

4. Conclusions

This work envisaged the production of a part made with AISI 410 stainless steel through WAAM, which was successfully achieved. The manufacturing of this part was accomplished through an initial stage of parametrization work and a second stage of deposition strategy fine tuning. Material characterization tests were also carried out, with the results being consistent with the expected ones. The following conclusions can be taken from this study: The main factor that influences the geometry of linear weld beads is the TS of the torch; Parameters that produce sound linear walls do not necessarily produce acceptable walls produced using an oscillation deposition path; Microstructure and macrostructure were in alignment with the literature, with no microstructural defects; Hardness values were in agreement with the ones found in literature, and characteristic of a martensitic structure; Tensile testing revealed high values for both UTS and YS in both directions. It also showed mild ductility in a transversal direction (Z-direction) and significant ductility in the longitudinal direction (X-direction); Comparing both software’s, WAAMPlanner appears to be the top choice as of now. Offering more control over segmentation of the part and process parameters, WAMMPlanner showed better performance at part depositing than Autodesk’s PowerMill Additive; WAAM software still has issues that need addressing. More strategies, especially weaving, could be available beyond oscillation and more freedom in path planning is required. A material database could also be beneficial in order to simplify the deposition process; Although process parameters have a considerable influence in part quality, an appropriate deposition strategy must be defined in order to achieve successful deposition; Heat accumulation also plays a role during deposition, and temperature between layers should be controlled in order to avoid defects.

As for deposition strategies the following aspects should be taken into account: As stated before, a combination of process parameters and deposition path must be achieved in order

to successfully produce a part; Minimizing the number of start and stops of the torch is also advisable, in order to reduce the number of segments and connection points; Deposition paths should take into account the limitations of the motion system.

5. References

[1] M. Attaran, “The rise of 3-D printing: The advantages of additive manufacturing over traditional manufacturing,” *Bus. Horiz.*, vol. 60, no. 5, pp. 677–688, 2017.

[2] D. Ding, Z. Pan, D. Cuiuri, and H. Li, “Wire-feed additive manufacturing of metal components: technologies, developments and future interests,” *Int. J. Adv. Manuf. Technol.*, vol. 81, no. 1–4, pp. 465–481, 2015.

[3] S. W. Williams, A. C. Addison, F. Martina, G. Pardal, J. Ding, and P. Colegrove, “Wire + Arc Additive Manufacturing,” *Mater. Sci. Technol.*, vol. 32, no. 7, pp. 641–647, 2015.

[4] M. M. Amrei, H. Monajati, D. Thibault, Y. Verreman, L. Germain, and P. Bocher, “Microstructure characterization and hardness distribution of 13Cr4Ni multipass weld metal,” *Mater. Charact.*, vol. 111, pp. 128–136, 2016.

[5] T. Wang, Y. Zhang, Z. Wu, and C. Shi, “Microstructure and properties of die steel fabricated by WAAM using H13 wire,” *Vacuum*, vol. 149, pp. 185–189, 2018.

[6] X. Xu, J. Ding, S. Ganguly, C. Diao, and S. Williams, “Oxide accumulation effects on wire + arc layer-by-layer additive manufacture process,” *J. Mater. Process. Technol.*, vol. 252, no. July 2017, pp. 739–750, 2018.

[7] T. A. Rodrigues, V. Duarte, R. M. Miranda, T. G. Santos, and J. P. Oliveira, “Current status and perspectives on wire and arc additive manufacturing (WAAM),” *Materials (Basel).*, vol. 12, no. 7, 2019.

[8] Y. M. Zhang, Y. Chen, P. Li, and A. T. Male, “Weld deposition-based rapid prototyping: A preliminary study,” *J. Mater. Process. Technol.*, vol. 135, no. 2-3 SPEC., pp. 347–357, 2003.

[9] Z. Hu, X. Qin, T. Shao, and H. Liu, “Understanding and overcoming of abnormity at start and end of the weld bead in additive manufacturing with GMAW,” *Int. J. Adv. Manuf. Technol.*, vol. 95, no. 5–8, pp. 2357–2368, 2018.

[10] S. Suryakumar, K. P. Karunakaran, A. Bernard, U. Chandrasekhar, N. Raghavender, and D. Sharma, “Weld bead modeling and process optimization in Hybrid Layered Manufacturing,” *CAD Comput. Aided Des.*, 2011.

[11] J. Xiong, G. Zhang, J. Hu, and L. Wu, “Bead geometry prediction for robotic GMAW-based rapid manufacturing through a neural network and a second-order regression analysis,” *J. Intell. Manuf.*, 2014.

[12] J. Xiong, G. Zhang, H. Gao, and L. Wu, “Modeling of bead section profile and overlapping beads with experimental validation for robotic GMAW-based rapid manufacturing,” *Robot. Comput. Integr. Manuf.*, 2013.

[13] X. Xu, J. Ding, S. Ganguly, C. Diao, and S. Williams, “Preliminary Investigation of Building Strategies of Maraging Steel Bulk Material Using Wire + Arc Additive Manufacture,” *J. Mater. Eng. Perform.*, pp. 1–7, 2018.

[14] D. Ding, Z. Pan, D. Cuiuri, and H. Li, “A tool-path generation strategy for wire and arc additive manufacturing,” *Int. J. Adv. Manuf. Technol.*, vol. 73, no. 1–4, pp. 173–183, 2014.

[15] J. Kao and F. B. Prinz, “OPTIMAL MOTION PLANNING FOR DEPOSITIONIN LAYERED MANUFACTURING,” 1998.

[16] G. Venturini, F. Montevecchi, A. Scippa, and G. Campatelli, “Optimization of WAAM Deposition Patterns for T-crossing Features,” *Procedia CIRP*, vol. 55, pp. 95–100, 2016.

[17] M. C. Tsai, C. S. Chiou, J. S. Du, and J. R. Yang, “Phase transformation in AISI 410 stainless steel,” *Mater. Sci. Eng. A*, vol. 332, no. 1–2, pp. 1–10, 2002.

[18] M. Divya, C. R. Das, V. Ramasubbu, S. K. Albert, and A. K. Bhaduri, “Improving 410NiMo weld metal toughness by PWHT,” *J. Mater. Process. Technol.*, vol. 211, no. 12, pp. 2032–2038, 2011.